determining step subsequent to the MLCT state.

The overall low efficiency of the reaction probably occurs in the formation of the key intermediate (ϕ_I) rather than in the silver-assisted product-forming step since it appears unlikely that a Ag^+-enhanced decay process leads back to the starting material from either of the intermediates reaction in eq 20/ or 21. The kinetic treatment indicates that the capture/decay ratio $k_r/k'_d = 17\ M^{-1}$ is relatively favorable; however, since it gives only a ratio, it is not possible to determine either the lifetime of the intermediate or the rate of capture from these experiments. Jonah, Matheson and Meisels[22] have performed pulse radiolysis studies on $Ru(bpy)_3^{3+}$ in aqueous solution where the key reaction observed is reduction of the trication by e_{aq}^-. In these studies formation of $Ru(bpy)_3^{2+}$ in the ground state as well as the MLCT state was observed as well as an additional process giving rise somewhat more slowly ($k \approx 10^4\ s^{-1}$)[22] to $Ru(bpy)_3^{2+}$ by an as yet unidentified intermediate. If we assume, as has been suggested,[11] that this intermediate is $Ru(bpy)_2bpy'(H_2O)^{2+}$ and that this is the species trapped by Ag^+ via eq 20 we can estimate that $k_r = k_{20} \approx 2 \times 10^5\ M^{-1}\ s^{-1}$. However, it could be argued that the use of a decay constant determined for aqueous solution is not appropriate since no Ag^+-assisted photosubstitution occurs in water.

A perhaps more plausible explanation for the observed results is that the Ag^+-assisted photosubstition involves reaction of the partially solvated intermediate $Ru(bpy)_2(bpy')(CH_3CN)$ (eq 21). Acetonitrile should be a reasonable ligand for the labilized metal center and it is likely that the aforementioned species might have an appreciable lifetime such that even relatively slow interception by Ag^+ could compete with decay.

The metal-cation-assisted photosubstitution described here is a potentially useful process which could prove to be quite general. Thus, even though the present process occurs with a low quantum efficiency its chemical yield is quite high. We plan to extend these studies to other solvent–metal ion systems as well as other transition-metal complexes.

Acknowledgment. We are grateful to the National Science Foundation (Grant No. CHE-7823126) for support of this research. João B. S. Bonilha (Visiting Scholar from Department of Chemistry, Faculdade de Filosofia Ciencias e Letras de Ribeirão Preto da Universidade de Sao Paulo, 14100-Ribeirão Preto S. P.-Brasil) acknowledges research fellowship support from the Fundaçao de Amparo à Pesquisa do Estado de Sao Paulo (FAPESP 16-quimica 80/0292) and research fellowship support from the Conselho Nacional de Desenvolvimento Cientifico e Tecnologico (CNPq 200.555-81-QU). We thank Professor T. J. Meyer for helpful discussions.

(22) Jonah, C. D.; Matheson, M. S.; Meisels, D. *J. Am. Chem. Soc.* **1978**, *100*, 1449.

Kinetics of the Reaction O + HO_2 → OH + O_2 from 229 to 372 K

Leon F. Keyser

Molecular Physics and Chemistry Section, Jet Propulsion Laboratory, California Institute of Technology, Pasadena, California 91109
(Received: February 16, 1982; In Final Form: April 23, 1982)

The discharge-flow resonance fluorescence technique has been used to obtain absolute rate data for the O + HO_2 reaction from 229 to 372 K at a total pressure of 1 torr. Pseudo-first-order conditions were used with HO_2 concentrations in large excess over initial atomic oxygen in order to minimize interference from secondary reactions. The results are independent of the method used to generate HO_2 and atomic oxygen. At 299 K, the result is $(6.1 \pm 0.4) \times 10^{-11}$ cm^3 molecule^{-1} s^{-1}. The temperature dependence expressed in Arrhenius form is $(3.1 \pm 0.3) \times 10^{-11} \exp[(+200 \pm 28)/T]$. The error limits given are twice the standard deviation; overall experimental error is estimated to be ±25%.

Introduction

The reaction of atomic oxygen with the hydroperoxyl radical (eq 1) plays an important role in the chemistry of

$$O + HO_2 \rightarrow OH + O_2 \quad (1)$$

the mesosphere and upper stratosphere.[1-4] Reaction 1 along with reaction 2 are the major paths by which odd

$$O + OH \rightarrow O_2 + H \quad (2)$$

oxygen (O, O_3) is converted to O_2 in these regions of the atmosphere. In addition, the rate constant ratio, k_1/k_2, is an important factor in determining the relative concentrations of OH and HO_2. Reaction 1 is also an important chain-breaking step in combustion chemistry.

There have been several earlier determinations of the rate constant, k_1, at 298 K with values ranging from 2.5×10^{-11} to 7×10^{-11} cm^3 molecule^{-1} s^{-1}.[5-7] No previous study of the temperature dependence of k_1 has been reported.

In the present study absolute measurements of k_1 have been made from 229 to 372 K by using resonance fluorescence detection of radical and atomic species. Pseudo-first-order conditions were used with [HO_2] >> [O]. The rate constant was determined directly from the slopes of [O] vs. time plots. At 299 K the result is (6.1 ±

(1) Nicolet, M. *Rev. Geophys. Space Phys.* **1975**, *13*, 593.
(2) Allen, M.; Yung, Y. L.; Waters, J. W. *J. Geophys. Res.* **1981**, *86*, 3617.
(3) Prather, M. J. *J. Geophys. Res.* **1981**, *86*, 5325.
(4) Logan, J. A.; Prather, M. J.; Wofsy, S. C.; McElroy, M. B. *Phil. Trans. R. Soc., Ser. A* **1978**, *290*, 187.
(5) Hack, W.; Preuss, A. W.; Temps, F.; Wagner, H. Gg. *Ber. Bunsenges. Phys. Chem.* **1979**, *83*, 1275.
(6) Burrows, J. P.; Cliff, D. I.; Harris, G. N.; Thrush, B. A.; Wilkinson, J. P. T. *Proc. R. Soc. London, Ser. A* **1979**, *368*, 463.
(7) Lii, R. R. Sauer, M. C., Jr.; Gordon, S. *J. Phys. Chem.* **1980**, *84*, 817.

0022-3654/82/2086-3439$01.25/0

0.4) × 10^{-11} cm^3 molecule^{-1} s^{-1}. A moderately negative temperature dependence was observed. At 229 K k_1 increases to (7.6 ± 0.5) × 10^{-11} cm^3 molecule^{-1} s^{-1}.

Experimental Section

The low-pressure flow system has been described in detail previously.[8,9] For the present study a dual resonance fluorescence cell was added downstream of the reaction zone. This system allows simultaneous detection of two radical species, in this case OH and atomic oxygen, at the same absolute reaction time. The present detector configuration greatly improves sensitivity and simplifies comparison of experimental concentration vs. time profiles with those generated from computer simulations.

All of the present measurements were carried out with a 50.4-mm diameter flow tube at temperatures between 229 and 372 K. Reactor surfaces were coated with a halocarbon wax (Series 15-00, Halocarbon Corp.). With this coating atomic oxygen wall loss was not observable (<1 s^{-1}); HO_2 loss was about 5 s^{-1}. Wall loss of OH was measured immediately before or after each calibration run. Between 372 and 229 K values without added NO ranged from 2 to 18 s^{-1} with an average value near 8 s^{-1}. With added NO, little or no change was observed in the OH wall loss for [OH] ≥ 10^{12} cm^{-3}. However, for [OH] in the 10^{11} cm^{-3} range the wall loss was found to increase by up to a factor of three when NO was added. Concentrations of NO near 3 × 10^{14} cm^{-3} were used in order to simulate conditions during the HO_2 to OH conversion (see discussion below). An increase in OH wall loss in the presence of NO has been observed previously with boric acid or phosphoric acid coated surfaces.[10,11]

HO_2 Sources. HO_2 radicals were generated in a movable reactor by adding atomic fluorine to an excess of H_2O_2

$$F + H_2O_2 \rightarrow HF + HO_2$$

This source has been described in detail previously.[8]

HO_2 radicals were also produced by reacting atomic chlorine with an excess of CH_3OH and O_2

$$Cl_2 \rightarrow 2Cl$$

$$Cl + CH_3OH \rightarrow HCl + CH_2OH \quad (17)$$

$$CH_2OH + O_2 \rightarrow CH_2O + HO_2 \quad (27)$$

k_{17} = 6.3 × 10^{-11} cm^3 molecule^{-1} s^{-1} [12] and k_{27} = 2 × 10^{-12} cm^3 molecule^{-1} s^{-1}.[13] The reactor used was similar in design to that used for the F + H_2O_2 source. Atomic chlorine was produced in a microwave discharge of a dilute Cl_2 in helium mixture. An uncoated quartz tube was used for the atomic chlorine production. Downstream of the discharge region the tube was coated with halocarbon wax. Production efficiencies of HO_2 based on the amounts of Cl_2 added varied from 30 to 70%. Under typical conditions the total flow was 1.37 L atm min^{-1} (293 K) at a pressure of about 1.5 torr. In the source, concentrations of CH_3OH and O_2 were about 9 × 10^{13} and 4 × 10^{15} cm^{-3}, respectively. At these concentrations reactions 17 and 27 were complete in the 2-ms reaction time before expansion into the main flow tube. The ratio of concentrations in the HO_2 source to those in the main reaction zone was approximately 2.5:1. This source was used to generate HO_2 concentrations in the main reaction zone between 6 × 10^{11} and 3 × 10^{12} cm^{-3}. Background concentrations of OH were found to be less than 1 × 10^{10} cm^{-3} with atomic oxygen less than 3 × 10^9 cm^{-3}.

Atomic Oxygen Sources. Atomic oxygen was produced at a fixed point upstream of the main reaction zone by dissociating O_2 in a microwave discharge or by the pyrolysis of O_3. Dissociation efficiencies between 12 and 21% were obtained by passing dilute mixtures of O_2 in helium through a microwave discharge operated at 50 W. Atomic oxygen was generated at concentrations between 5 × 10^{10} and 1.2 × 10^{11} cm^{-3} with OH concentrations less than 2 × 10^9 cm^{-3} and atomic hydrogen less than 4 × 10^9 cm^{-3}.

An alternate source of atomic oxygen was the thermal decomposition of ozone. Dilute mixtures of O_3 in helium were passed through a quartz tube placed in an electric furnace. At temperatures between 975 and 1015 K, an atomic oxygen production yield of about 25% was obtained in a 8.5-ms residence time. Concentrations of atomic oxygen were between 4 × 10^{10} and 2 × 10^{11} cm^{-3} with background OH less than 1 × 10^9 cm^{-3}.

HO_2 to OH Conversion. HO_2 was determined by quantitatively converting it to OH with an excess of NO (eq 39). The fixed NO addition port was located 2–3-ms

$$HO_2 + NO \rightarrow OH + NO_2 \quad (39)$$

upstream of the OH detector. Two methods of NO addition were used: (a) a single 1-mm orifice located at the center of the flow tube and (b) eight 1-mm orifices located on a 2.6-cm diameter circle. In both cases the NO flow was opposed to the main helium flow in order to increase the mixing efficiency. There was no significant difference in the observed value of k_1 (obtained from atomic oxygen decay rates and absolute HO_2 concentrations) when either method of NO addition was used. This is evidence that NO mixing was sufficiently complete and, thus, did not affect the HO_2 concentration measurements.

Detector Calibrations. OH was monitored by resonance fluorescence near 308 nm. The calibration procedure was similar to that used previously.[8] Known concentrations of OH were generated by reacting NO_2 with excess H atoms (eq 30). The NO_2 was added through a movable inlet

$$H + NO_2 \rightarrow OH + NO \quad (30)$$

located approximately 9-ms upstream of the OH detector. Typical concentrations used were [H] = 1.7 × 10^{13} cm^{-3} with [NO_2] between 1 × 10^{12} and 3 × 10^{12} cm^{-3}.

It was found that OH calibration signals decreased 5–10% when NO was added through the fixed inlet 2–3-ms upstream of the OH detector at concentrations similar to those used in the HO_2 to OH conversion. This reduction was too large to be accounted for entirely by increased wall loss or dilution by NO. It was possibly due to reaction 36

$$OH + NO + He \rightarrow HONO + He \quad (36)$$

or to quenching of OH fluorescence before complete mixing of NO occurs. Evidence that this was related to NO mixing was the observation of a lower loss (~5%) when the more efficient eight-orifice NO addition port was used compared to a loss of 8–10% with the one-orifice port.

To minimize calibration errors, we allowed reaction 30 to proceed for approximately 7 ms. NO was then added at concentrations between 2.5 × 10^{14} and 3.2 × 10^{14} cm^{-3}. Concentrations of OH were corrected for losses due to reaction 5 (2–8%) by using k_5 = 1.8 × 10^{-12} cm^3 molecule^{-1}

$$OH + OH \rightarrow H_2O + O \quad (5)$$

s^{-1} and for wall loss (2–16%, with a typical value about 5%)

(8) Keyser, L. F. *J. Phys. Chem.* **1981**, *85*, 3667.
(9) Keyser, L. F. *J. Phys. Chem.* **1980**, *84*, 1659.
(10) Anderson, J. G.; Margitan, J. J.; Kaufman, F. *J. Chem. Phys.* **1974**, *60*, 3310.
(11) Howard, C. J.; Evenson, K. M. *J. Chem. Phys.* **1974**, *61*, 1943.
(12) Michael, J. V.; Nava, D. F.; Payne, W. A.; Stief, L. J. *J. Chem. Phys.* **1979**, *70*, 3652.
(13) Radford, H. E. *Chem. Phys. Lett.* **1980**, *71*, 195.

by using measured values of k_{wall}. These corrections were made only for the 7-ms reaction time up to the NO addition port. Downstream of this point losses due to reactions 5 and 36 and wall losses were also present during the HO_2 to OH conversion (see discussion on absolute HO_2 concentrations below) and no corrections for these losses were needed. This procedure yielded an OH detector sensitivity, $S(OH)$, which was based on the OH concentration at the NO addition port, $[OH]_p$ (eq I). In this expression I_c is the fluorescence intensity observed during the calibration run.

$$S(OH) = I_c/[OH]_p \quad (I)$$

Atomic oxygen and hydrogen were monitored by resonance fluorescence at 130.6 and 121.6 nm, respectively. Oxygen atom fluorescence was calibrated by adding a known amount of NO to an excess of N atoms.

$$N + NO \rightarrow N_2 + O$$

The observed fluorescence signals were tested for linearity vs. atomic oxygen concentrations by using eq II, where I

$$I = \alpha[O]^n \quad (II)$$

is the atomic oxygen fluorescence intensity; and α is a constant proportional to the exciting light intensity, the detector sensitivity, and collection efficiency. The exponent n was used to assess the degree of linearity. Least-squares analysis shows that $n = 0.97 \pm 0.01$ up to $[O] = 1.8 \times 10^{11}$ cm^{-3}. Thus, the fluorescence was linear within 3% over the atomic oxygen concentration range used in this study.

Atomic hydrogen signals were calibrated by converting the H atoms to OH by adding an excess of NO_2 (eq 30). The OH fluorescence had been previously calibrated as described above.

Reagents. Gases used were chromatographic grade helium (99.9999%), research grade hydrogen (99.9995%), ultrahigh-purity oxygen (99.95%), ultrahigh-purity nitrogen (99.999%), nitric oxide (99.0%), and a 0.5% mixture of fluorine in helium. The nitric oxide was purified by passage through a molecular sieve (Linde 13X) trap at 195 K. Nitrogen dioxide was prepared from nitric oxide by adding a large excess of oxygen. After several hours the oxygen was removed by slowly passing the mixture through a 195-K trap. The nitrogen dioxide was stored at 77 K and distilled to a 195-K trap before use. The fluorine in helium mixture was passed through a 77-K trap, and the chromatographic helium was passed through a molecular sieve (Linde 3A) trap at 77 K just prior to use. Hydrogen peroxide (90%) was obtained from FMC. It was concentrated to greater than 95% by pumping. Concentrations of hydrogen peroxide were determined as described previously.[9] Ozone was produced by discharging oxygen in a Welsbach Model T-816 ozonator and trapped at 195 K on silica gel. Concentrations of ozone were measured as discussed earlier.[14] Methanol (reagent grade) was added by passing a stream of helium through the liquid in a constant temperature reservoir. Concentrations were calculated by using the vapor pressure of methanol, the helium flow rate, and total pressure.

Results

The present experiments were carried out at temperatures between 229 and 372 K at a total pressure of (1.02 ± 0.02) torr of helium. HO_2 concentrations were 6.5×10^{11}–3.3×10^{12} cm^{-3} with initial atomic oxygen concentrations of 5.0×10^{10}–1.9×10^{11} cm^{-3}. Initial stoichiometric ratios, $[HO_2]/[O]_0$, were 5–46 with a value greater than 15 being typical. Under these conditions the loss of atomic oxygen is pseudo-first-order and may be written

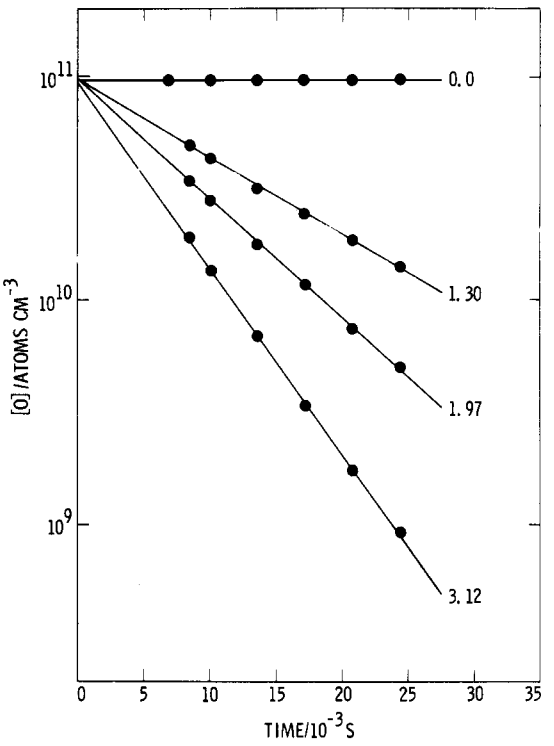

Figure 1. Pseudo-first-order decays of atomic oxygen at 264 K. The numbers adjacent to each decay curve give $[HO_2]$ in units of 10^{12} cm^{-3}. The lines through the data points are linear least-squares fits.

$$k_+^I = -(d \ln [O]/dt)_+ = k_1[HO_2] + k_L \quad (III)$$

where k_+^I represents the pseudo-first-order rate constant for loss of atomic oxygen with HO_2 present in the system (movable discharge on). In general, a term $k_2[OH]$ should be included on the right-hand side of eq III since OH is a product of reaction 1. However, under the conditions of the present experiments, the observed [OH] was less than 5×10^{10} cm^{-3} and $k_2[OH]$ is negligible compared to $k_1[HO_2]$. This is confirmed by computer simulations discussed below. All losses of atomic oxygen other than by reactions 1 and 2 are grouped in the k_L term which would include, for example, reactions with H_2O_2 or CH_3-OH. When HO_2 is not present (movable discharge off) the loss is

$$k_-^I = -(d \ln [O]/dt)_- = k_L \quad (IV)$$

and

$$k^I = k_+^I - k_-^I = k_1[HO_2] \quad (V)$$

Equating k_-^I and k_L in eq IV assumes that atomic oxygen losses due to secondary reactions are negligibly changed when the HO_2 source is switched on and off. Evidence that the secondary chemistry is unimportant is provided by using two entirely different sources of HO_2 and will be discussed below.

Typical atomic oxygen decays for several HO_2 concentrations at 264 K are shown in Figure 1. No loss was observed in the absence of HO_2 ($k_-^I < 1$ s^{-1}) except at 372 K where $k_-^I = 2.5$ s^{-1}. Generally, the decay plots showed no evidence of curvature over two or more reaction lifetimes. The slopes were used to obtain k^I.

Table I summarizes the experimental conditions and results obtained in the present study. Concentrations of

(14) Keyser, L. F. *J. Phys. Chem.* **1979**, *83*, 645.

TABLE I: Kinetic Data for $O + HO_2 \rightarrow OH + O_2$

temp, K	$\bar{v}$, cm s^{-1}	radical sources	$10^{-12} \times [HO_2]$, cm^{-3}	$10^{-10} \times [O]_0$, cm^{-3}	k^I, s^{-1}	$10^{11}k_1$, cm^3 molecule^{-1} s^{-1}
372	1770	*a*	0.959	8.59	50.9	5.31
			1.57	9.02	81.2	5.17
			1.88	8.74	101.4	5.39
			2.08	9.60	107.7	5.18
			2.35	11.6	130.8	5.57
			2.66	14.2	148.5	5.58
						av (5.37 ± 0.36)[d]
299	1530	*a*	1.07	6.83	60.3	5.64
			1.32	3.80	77.8	5.89
			1.61	13.9	94.8	5.89
			1.62	5.02	93.2	5.75
			1.95	6.91	114.7	5.88
			1.96	7.25	122.4	6.24
			2.01	13.1	119.1	5.92
			2.22	7.11	136.2	6.14
			2.34	12.9	145.1	6.20
			2.63	14.7	161.2	6.13
			2.83	7.50	158.4	5.60
			3.20	6.88	198.7	6.21
			3.20	13.9	196.6	6.14
			3.32	7.27	209.5	6.31
						av (6.00 ± 0.46)[d]
299	1520	*b*	0.853	9.47	50.4	5.91
			0.973	8.25	56.6	5.82
			1.18	5.92	70.4	5.97
			1.24	11.1	78.3	6.32
			1.44	10.5	88.8	6.17
			1.45	18.8	93.9	6.48
			1.64	11.0	105.7	6.44
			1.65	7.12	105.6	6.40
			1.84	17.1	120.1	6.53
			2.18	6.36	135.4	6.21
			2.19	10.4	138.9	6.34
			2.45	9.58	149.1	6.09
			2.56	15.6	169.2	6.61
			2.83	18.7	187.0	6.61
			3.10	11.3	196.5	6.34
						av (6.28 ± 0.50)[d]
299	1500	*c*	0.653	12.37	35.8	5.48
			0.717	5.44	45.6	6.36
			0.911	7.59	59.2	6.50
			1.06	6.49	70.1	6.61
			1.17	6.88	70.2	6.00
			1.18	5.67	68.5	5.80
			1.37	6.48	78.7	5.74
			1.46	5.56	81.0	5.55
			1.58	7.87	94.7	5.99
			1.67	6.26	98.1	5.87
			1.79	8.17	105.4	5.89
			1.81	8.86	112.6	6.22
			1.91	5.55	120.4	6.30
			1.92	6.48	111.1	5.79
			2.01	7.92	111.1	5.53
			2.18	6.20	125.1	5.74
			2.20	6.72	139.8	6.36
			2.36	7.80	142.8	6.05
			2.38	9.28	145.2	6.10
			2.63	7.37	188.4	7.16
			2.92	7.20	170.9	5.85
						av (6.04 ± 0.82)[d]
264	1400	*a*	1.30	9.45	83.1	6.39
			1.69	10.4	109.6	6.48
			1.97	9.39	130.0	6.60
			2.59	8.86	166.1	6.41
			2.89	15.1	189.4	6.55
			3.12	8.63	210.9	6.76
						av (6.53 ± 0.28)[d]
229	1220	*a*	0.974	12.3	73.5	7.55
			1.63	12.8	128.7	7.90
			1.73	11.7	134.0	7.75
			2.06	13.7	153.8	7.47
			2.18	13.2	157.4	7.22

TABLE I (*Continued*)

temp, K	v, cm s^{-1}	radical sources	$10^{-12} \times [HO_2]$, cm^{-3}	$10^{-10} \times [O]_0$, cm^{-3}	k^I, s^{-1}	$10^{11}k_1$, cm^3 $molecule^{-1}$ s^{-1}
			2.38	13.2	179.3	7.53
						av (7.57 ± 0.46)[d]

[a] Atomic oxygen from ozone pyrolysis; HO_2 from Cl + CH_3OH + O_2. [b] Atomic oxygen from ozone pyrolysis; HO_2 from F + H_2O_2. [c] Atomic oxygen from microwave discharge of O_2; HO_2 from F + H_2O_2. [d] Errors are twice the standard deviation.

TABLE II: Rate Constants for the O + HO_2 Reaction

temp, K	radical sources	$10^{11}k_1$,[d] cm^3 $molecule^{-1}$ s^{-1} average[e]	slope[f]	intercept,[f] s^{-1}
372	*a*	5.37 ± 0.36	5.77 ± 0.52	−7 ± 10
299	*a*	6.00 ± 0.46	6.39 ± 0.38	−8 ± 9
299	*b*	6.28 ± 0.50	6.62 ± 0.30	−5 ± 6
299	*c*	6.04 ± 0.82	6.28 ± 0.58	−4 ± 10
	overall average at 299 K:	6.11 ± 0.36		
264	*a*	6.53 ± 0.28	6.82 ± 0.41	−6 ± 10
229	*a*	7.57 ± 0.46	7.19 ± 0.80	+7 ± 15

[a] Atomic oxygen from ozone pyrolysis; HO_2 from Cl + CH_3OH + O_2. [b] Atomic oxygen from ozone pyrolysis; HO_2 from F + H_2O_2. [c] Atomic oxygen from microwave discharge of O_2; HO_2 from F + H_2O_2. [d] Errors are twice the standard deviation. [e] From average of individual $k^I/[HO_2]$ values. [f] From plot of k^I vs. $[HO_2]$; the values given are from linear least-squares fits.

HO_2 are the average of the concentrations observed at the minimum and maximum reaction times of each run. Observed HO_2 decays due to wall loss, recombination (eq 6),

$$HO_2 + HO_2 \rightarrow H_2O_2 + O_2 \qquad (6)$$

and reaction with atomic oxygen were generally less than 15%. The data have been corrected for axial and radial diffusion,[15] for the viscous pressure drop between the reaction zone and the pressure measurement port,[16] and for quenching of OH fluorescence by O_2. Pressure corrections lowered the observed values of k_1 by less than 2% while diffusion corrections increased k_1 from 2 to 10%. Quenching corrections were made by using a radiative lifetime of 0.693 μs for the A state of OH[17] and a value of 9.6×10^{-11} cm^3 $molecule^{-1}$ s^{-1} for the O_2 quenching rate constant.[18,19] The latter corrections, which were necessary only when HO_2 was produced by Cl + CH_3OH + O_2, decreased observed k_1 values by about 12%. Corrections for radical losses during the HO_2 to OH conversion (see Discussion section) have also been applied to the HO_2 concentrations given in column one. These corrections decreased the observed k_1 values by 4–14%. Net corrections to k_1 averaged about 15% or less which is well within the estimated experimental error of ±25%.

The last column of Table I gives the bimolecular rate constant, k_1, obtained from $k^I/[HO_2]$. Plots of k^I vs. $[HO_2]$ were also used to calculate k_1, and the results are summarized in Table II. The averages of $k^I/[HO_2]$ values differ by less than twice the standard deviation from values calculated from the least-squares slopes. Average values are used in the remainder of this discussion.

The rate data are plotted in Arrhenius form in Figure 2. The resulting Arrhenius expression obtained from a linear least-squares analysis of the data is

$$k_1 \text{ (cm}^3 \text{ molecule}^{-1} \text{ s}^{-1}) = (3.1 \pm 0.3) \times 10^{-11} \exp[(+200 \pm 28)/T]$$

for $229 \leq T \leq 372$ K. The errors are twice the standard deviation obtained from the analysis.

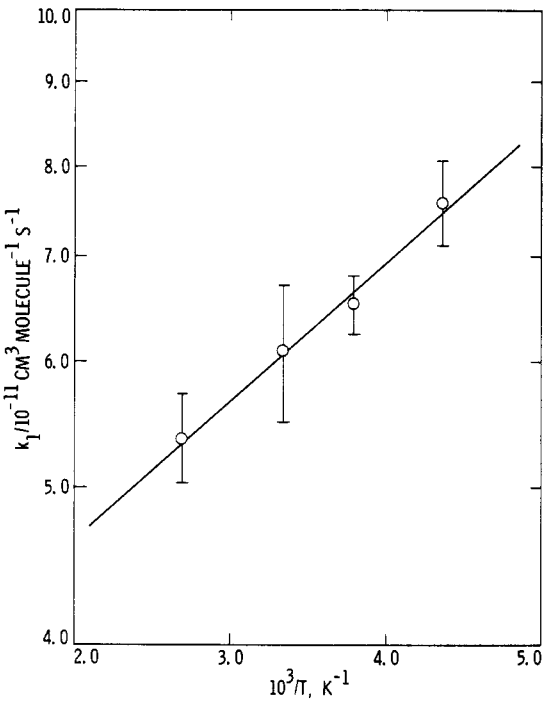

Figure 2. Arrhenius plot of the rate data for O + HO_2. The error bars are twice the standard deviation.

Discussion

Secondary Chemistry. At the high initial stoichiometric ratios used in the present study, secondary reactions involving product OH should be negligible. This is confirmed by the absence of curvature in atomic oxygen pseudo-first-order decay plots and by the lack of any significant variation in k_1 over a wide range of initial concentrations. Moreover, the results are essentially independent of the sources of atomic oxygen and HO_2. This shows that the secondary chemistry associated with the sources is also unimportant.

As an additional test for interference from secondary reactions, computer simulations of the k_1 determinations were run with the reactions listed in Table VI of the Appendix. For HO_2 produced from F + H_2O_2 and atomic

(15) Brown, R. L. *J. Res. Natl. Bur. Stand. (U.S.)* **1978**, *83*, 1, and references cited therein.
(16) Kaufman, F. *Prog. React. Kinet.* **1961**, *1*, 1.
(17) German, K. R. *J. Chem. Phys.* **1975**, *63*, 5252.
(18) German, K. R. *J. Chem. Phys.* **1976**, *64*, 4065.
(19) Selzer, P. J.; Wang, C. C. *J. Chem. Phys.* **1979**, *71*, 3786.

TABLE III: Results of Test for Secondary Reactions Using Computer Simulations[a]

$10^{-12} \times [HO_2]_0$, cm^{-3}	$10^{-11} \times [O]_0$, cm^{-3}	$10^{11}k_1$(calcd),[b] cm^3 molecule^{-1} s^{-1}	k_1(model)[c]/k_1(calcd)
1.0	0.5	6.16	0.99
1.0	1.0	6.23	0.98
2.0	1.0	6.11	1.00
3.0	1.0	6.11	1.00

[a] HO_2 from Cl + CH_3OH + O_2; O atoms from O_3 pyrolysis; reactions 1-3 and 5-29 of Table VI. $[OH]_0 = 5 \times 10^9$ cm^{-3}, $[H]_0 = 5 \times 10^9$ cm^{-3}, $[O_3] = (2\text{-}4) \times 10^{11}$ cm^{-3}, $[CH_3OH] = 4 \times 10^{13}$ cm^{-3}, $[O_2] = 1.3 \times 10^{15}$ cm^{-3}. [b] k_1(calcd) is obtained from slope of computer-generated ln [O] vs. time plots for reaction times between 6 and 22 ms. [c] k_1(model) = 6.1×10^{-11} cm^3 molecule^{-1} s^{-1}.

oxygen from an O_2 discharge, reactions 1–10 were used; for HO_2 from F + H_2O_2 and atomic oxygen from O_3 pyrolysis, reactions 1–14 were used; and for HO_2 from Cl + CH_3OH + O_2 and atomic oxygen from O_3 pyrolysis, reactions 1–3 and 5–29 were used. In all cases initial concentrations were similar to those of experimental runs. A value of 6.1×10^{-11} cm^3 molecule^{-1} s^{-1} was used for k_1 in the model. The results obtained for the third case are summarized in Table III; similar results were obtained for the other simulations. The value of k_1(calcd) was obtained from the computer generated ln [O] vs. time plots for reaction times between 6 and 22 ms. This closely simulates the procedure used to obtain k_1 from actual experimental data. The last column gives the ratio of k_1 used in the model to k_1 calculated. The results confirm that secondary reactions do not interfere with the present measurements. Little or no curvature was detected in the computer-generated ln [O] vs. time plots in agreement with experimental observations.

Absolute HO_2 Concentrations. As discussed earlier HO_2 was determined after quantitatively converting it to OH by adding a large excess of NO (eq 39) 2–3-ms upstream of the OH detector. As the NO concentration was increased the observed signal intensity of OH generated from HO_2 increased to a broad maximum and then slowly decreased. Concentrations of NO used were near the maximum of the OH signal. For HO_2 generated from F + H_2O_2, $[NO] = 3.2 \times 10^{14}$ cm^{-3}; for HO_2 from Cl + CH_3OH + O_2, $[NO] = 2.5 \times 10^{14}$ cm^{-3}. Possible reasons for this difference will be discussed below.

During the conversion of HO_2 to OH, some loss of radicals is expected to occur mainly by reactions 3, 5, 10, and 36 (see Table VI). By calculating the OH detector sensitivity in terms of the OH concentration at the NO addition port (eq I), losses due to reactions 5, 10, and 36 which are present both during the calibration and the conversion tend to cancel and calibration errors are minimized.

To estimate the magnitude of radical loss, both the OH calibration and the HO_2 to OH conversion were simulated with computer models. For the OH calibration, reactions 2, 5, 10, and 30–38 in Table VI were used. Initial concentrations were chosen to simulate experimental runs with $[H]_0 = 1.7 \times 10^{13}$ cm^{-3}, $[H_2]_0 = 8.5 \times 10^{12}$ cm^{-3}, and $[NO_2]_0 = 1 \times 10^{12}\text{–}3 \times 10^{12}$ cm^{-3}. The results for $[NO_2]_0 = 2 \times 10^{12}$ cm^{-3} are shown in Figure 3. Correcting $[NO_2]_0$ with only reactions 5 and 10 yields OH concentrations at 7 ms which agree with the computer-generated values to within 1%. This correction procedure is exactly that used on the experimental data. The close agreement confirms that the major losses of OH during calibration have been included.

For the HO_2 to OH conversion, reactions 1–14, 30, 31, and 33–40 were used for the F + H_2O_2 system. All of the reactions given in Table VI except reactions 4 and 32 were used to model the Cl + CH_3OH + O_2 system. Initial concentrations were similar to those observed in actual experiments. Initial concentrations of HO_2 were those calculated from the OH calibration model at the 7-ms reaction time. The results for $[HO_2]_0 = 1.81 \times 10^{12}$ cm^{-3} and $[NO] = 3.2 \times 10^{14}$ cm^{-3} are shown in Figure 3. This initial concentration of HO_2 is equal to the concentration of OH at the 7-ms reaction time during the calibration run

TABLE IV: Computer Simulations of OH Calibration and HO_2 to OH Conversion

OH calibration			HO_2 to OH conversion		
$10^{-12} \times [NO_2]_0$, cm^{-3}	$10^{-12} \times [OH]_{7ms}$,[a] cm^{-3}	$10^{-12} \times [OH]_{9ms}$,[b] cm^{-3}	$10^{-12} \times [HO_2]_0$, cm^{-3}	$10^{-12} \times [OH]_{2ms}$,[c,e] cm^{-3}	corr factor[d,e]
1.0	0.927	0.843	0.927	0.814 (0.789)	1.04 (1.07)
2.0	1.81	1.63	1.81	1.54 (1.48)	1.06 (1.10)
3.0	2.64	2.36	2.64	2.20 (2.09)	1.07 (1.13)

[a] $[OH]_{7ms}$ is OH concentration 7 ms after start of H + NO_2 reaction. [b] $[OH]_{9ms}$ is OH concentration 9 ms after start of H + NO_2 reaction and 2 ms after NO addition. [c] $[OH]_{2ms}$ is OH concentration 2 ms after start of HO_2 + NO reaction. [d] Correction factor is $[OH]_{9ms}/[OH]_{2ms}$. [e] Numbers without parentheses give results for HO_2 from F + H_2O_2. Numbers in parentheses give results for HO_2 from Cl + CH_3OH + O_2. For F + H_2O_2 source: $[H_2O_2] = 3.1 \times 10^{13}$ cm^{-3}; $[NO] = 3.2 \times 10^{14}$ cm^{-3}; $[O_3] = 4.0 \times 10^{11}$ cm^{-3}; no difference was observed when $[O_3] = 0$. For Cl + CH_3OH + O_2 source: $[CH_3OH] = 4.0 \times 10^{13}$ cm^{-3}; $[NO] = 2.5 \times 10^{14}$ cm^{-3}; $[O_3] = 4.0 \times 10^{11}$ cm^{-3}; $[O_2] = 1.7 \times 10^{15}$ cm^{-3}.

TABLE V: Summary of k_1 Measurements at 298 K

$10^{11}k_1$, cm^3 molecule^{-1} s^{-1}	press, torr	runs	method[a]	comments	ref
6.1 ± 0.4	1.0	50	DF-RF	absolute measurement, $[HO_2] >> [O]$	present results
3.7[b] (3.3 ± 1.0)[c]	0.8-2.3	6	DF-LMR-ESR	results depend on k_3 and k_4, $[O] >> [HO_2]$	5
4.2 ± 1.5	2.8-3.4	4	DF-LMR-ESR	absolute measurement, $[HO_2] >> [O]$	5
3.0[d] (3.3 ± 1.0)[c]	3.7-5.5	5	DF-LMR-ESR	relative to k_2	5
2.7[d] (2.9 ± 1)[c]	1.0	8	DF-LMR	relative to k_2	6
6.3[e] (3.2 ± 1)[c]	1.0	8	DF-LMR	relative to k_4	6
7 ± 2	1200	6	PR-UVA	computer simulations of $[HO_2]$ and $[O_3]$ vs. time	7

[a] DF, discharge flow; RF, resonance fluorescence; LMR, laser magnetic resonance; ESR, electron spin resonance; PR, pulse radiolysis; UVA, ultraviolet absorption. [b] Recalculated by using $k_4 = 1.7 \times 10^{-12}$ cm^3 s^{-1} and $k_3 = 6.4 \times 10^{-11}$ cm^3 s^{-1}. [c] The numbers in parentheses are the originally reported values of k_1. [d] Based on $k_2 = 3.3 \times 10^{-11}$ cm^3 s^{-1}. [e] Based on $k_4 = 1.7 \times 10^{-12}$ cm^3 s^{-1}.

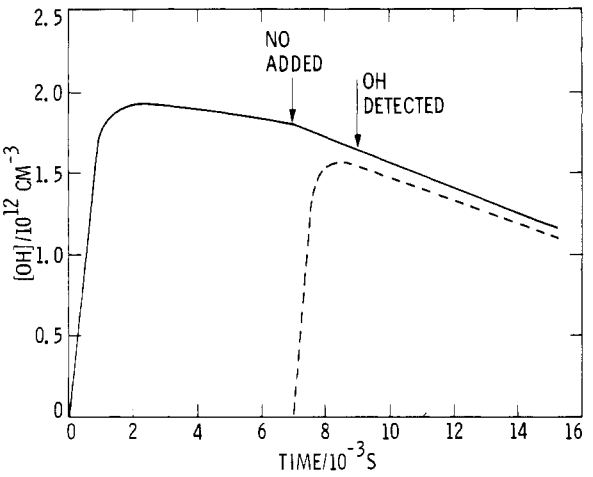

Figure 3. Computer simulations of OH calibration and HO_2 to OH conversion. The solid line shows [OH] during a calibration run with OH generated from H + NO_2 (eq 30). [H] = 1.7 × 10^{13} cm^{-3}, $[NO_2]_0$ = 2.0 × 10^{12} cm^{-3}, [NO] = 3.2 × 10^{14} cm^{-3}. The change in slope at the NO addition point is due to the increased OH loss in the presence of NO (see text). The dashed line gives [OH] during HO_2 to OH conversion with OH generated from HO_2 + NO (eq 39). $[HO_2]_0$ = 1.8 × 10^{12} cm^{-3}, [NO] = 3.2 × 10^{14} cm^{-3}.

which used an initial NO_2 concentration of 2.0 × 10^{12} cm^{-3}. The ratio of OH concentration at the detector during calibration to that during conversion gives an estimate of additional OH losses during the HO_2 to OH conversion. Results at several initial concentrations are summarized in Table IV, the last column of which gives the desired ratio. Additional HO_2 to OH conversion losses in the system with F + H_2O_2 as the HO_2 source are calculated to be less than 10%. Added losses in the system with Cl + CH_3OH + O_2 to form HO_2 are less than 15%. The slightly higher loss in the latter system is evidently due to formation of HNO by reaction of NO with HCO (eq 41) and possibly with CH_2OH (eq 42). Unlike HCO, HNO

$$HCO + NO \rightarrow HNO + CO \quad (41)$$

$$CH_2OH + NO \rightarrow HNO + H_2CO \quad (42)$$

does not react rapidly with O_2 to form HO_2. Thus, formation of HNO represents a loss of HO_x radicals from the system. This loss due to HNO formation also accounts for the occurrence of maximum OH from HO_2 at lower NO concentrations than those used in the F + H_2O_2 system.

Absolute HO_2 concentrations were obtained from the observed OH fluorescence intensities by using the calibrated detector sensitivity, $S(OH)$, defined in eq I. This gives the HO_2 concentration at the NO addition port uncorrected for added losses during the HO_2 to OH conversion. Correction factors derived in a manner similar to those in Table IV were then applied to obtain HO_2 concentrations used in the rate constant calculations. In all cases these corrections were less than 14%.

Comparison with Previous Results. Measurements of k_1 near 298 K are summarized in Table V. Some of the earlier studies were made relative to k_2 and k_4 or depend on values for k_3 and k_4. As discussed more fully below, the close agreement of two of the previous studies with the present result may be accidental.

Hack et al. made three determinations of k_1 using a discharge flow system with laser magnetic resonance–electron spin resonance detection.[5] In the first measurement, excess atomic oxygen was used. Under these conditions, the observed HO_2 decays ranged from 11 to 160 s^{-1} but included large contributions, 8–72 s^{-1}, due to HO_2 regeneration from reaction 4. Thus, this method is not suitable for an accurate determination of k_1. The second measurement of Hack et al. followed the decay of atomic oxygen in the presence of excess HO_2. The results are about 45% below the present results. The reason for the difference is not clear since similar conditions appear to have been used in both studies. A possible cause may lie in the details of the calibration procedure used to obtain absolute HO_2 concentrations. The third k_1 determination of Hack et al. was made relative to k_2 by measuring [OH] and $[HO_2]$ at the time that [OH] was at its maximum. OH was produced by reaction 1 and destroyed by reaction 2 and wall losses. Computer simulations of these experiments with conditions given in Table 3 of Hack et al. show that the [OH] maximum occurs in about 1 ms and that at this time the $[HO_2]$ is falling rapidly. Thus, a reliable

TABLE VI: Reactions Used in Computer Simulations

no.	reaction	rate constant at 298 K[a]
(1)	O + HO_2 → OH + O_2	6.1 × 10^{-11} [b]
(2)	O + OH → O_2 + H	3.3 × 10^{-11}
(3)	OH + HO_2 → H_2O + O_2	6.4 × 10^{-11} [c]
(4)	OH + H_2O_2 → H_2O + HO_2	1.7 × 10^{-12}
(5)	OH + OH → H_2O + O	1.8 × 10^{-12}
(6)	HO_2 + HO_2 → H_2O_2 + O_2	1.0 × 10^{-12}
(7)	H + HO_2 → OH + OH	3.2 × 10^{-11}
(8)	H + HO_2 → H_2 + O_2	1.4 × 10^{-11}
(9)	HO_2 + wall → products	5 s^{-1} [b]
(10)	OH + wall → products	8 s^{-1} [b,d]
(11)	O + O_3 → 2 O_2	8.8 × 10^{-15}
(12)	HO_2 + O_3 → OH + 2 O_2	1.6 × 10^{-15}
(13)	OH + O_3 → HO_2 + O_2	6.8 × 10^{-14}
(14)	H + O_3 → OH + O_2	2.8 × 10^{-11}
(15)	O + CH_3OH → OH + CH_2OH	5.5 × 10^{-15} [e]
(16)	OH + CH_3OH → H_2O + CH_2OH	1.1 × 10^{-12}
(17)	Cl + CH_3OH → HCl + CH_2OH	6.3 × 10^{-11} [f]
(18)	Cl + O_3 → ClO + O_2	1.2 × 10^{-11}
(19)	O + H_2CO → OH + HCO	1.6 × 10^{-13}
(20)	OH + H_2CO → H_2O + HCO	1.0 × 10^{-11}
(21)	H + H_2CO → H_2 + HCO	5.4 × 10^{-14}
(22)	Cl + H_2CO → HCl + HCO	7.3 × 10^{-11}
(23)	O + Cl_2 → ClO + Cl	4.2 × 10^{-14}
(24)	H + Cl_2 → HCl + Cl	2.0 × 10^{-11}
(25)	OH + Cl_2 → HOCl + Cl	5.5 × 10^{-14} [g]
(26)	Cl + HO_2 → HCl + O_2	4.8 × 10^{-11}
(27)	O_2 + CH_2OH → HO_2 + H_2CO	2.0 × 10^{-12} [h]
(28)	O + HCO → OH + CO	2.1 × 10^{-10}
(29)	O_2 + HCO → HO_2 + CO	5.0 × 10^{-12}
(30)	H + NO_2 → OH + NO	1.3 × 10^{-10}
(31)	O + NO_2 → O_2 + NO	9.3 × 10^{-12}
(32)	OH + H_2 → H_2O + H	7.5 × 10^{-15}
(33)	H + NO + He → HNO + He	2.0 × 10^{-32} [i]
(34)	OH + HNO → H_2O + NO	7.0 × 10^{-11}
(35)	H + HNO → H_2 + NO	1.0 × 10^{-13}
(36)	OH + NO + He → HONO + He	3.8 × 10^{-31} [i]
(37)	OH + NO_2 + He → $HONO_2$ + He	9.2 × 10^{-31} [i]
(38)	O + NO + He → NO_2 + He	6.2 × 10^{-32} [i]
(39)	HO_2 + NO → OH + NO_2	8.1 × 10^{-12}
(40)	O_3 + NO → NO_2 + O_2	1.8 × 10^{-14}
(41)	HCO + NO → HNO + CO	1.3 × 10^{-11} [j]
(42)	CH_2OH + NO → HNO + H_2CO	5.0 × 10^{-12} [k]

[a] Unless otherwise indicated, units are cm^3 $molecule^{-1}$ s^{-1} and values were obtained from ref 26–28. [b] Measured. [c] Reference 8. [d] In the absence of added NO k_{10} = 8 s^{-1}, the average of the observed wall loss. To account for the increased loss of OH in the presence of NO (not necessarily due to wall loss, see text), k_{10} = 40 s^{-1} when NO was added. At this value the reduction in [OH] with NO present amounts to about 6% in 2 ms which closely simulates the experimental observation. [e] Reference 29. [f] Reference 12. [g] Reference 30. [h] Reference 13. [i] cm^6 $molecule^{-2}$ s^{-1}. [j] References 31 and 32. [k] Estimated. The results are not very sensitive to the value of k_{42} used. For example, calculated OH loss during HO_2 to OH conversion is 6 and 9% for k_{42} = 0 and 5 × 10^{-11} cm^3 $molecule^{-1}$ s^{-1}, respectively.

measurement of k_1/k_2 cannot be made in this way. A better approach is to determine k_1/k_2 from the quasi-steady state [OH] and [HO_2] which occur at longer reaction times.

Burrows et al.[6] measured k_1 relative to k_2 and k_4 using a low-pressure flow system with laser magnetic resonance detection. Rate data were obtained from the observed maximum concentrations of OH and HO_2 radicals which were generated by reacting atomic oxygen with H_2O_2. The results when corrected by using recently reported measurements of k_4[9,20,21] become internally inconsistent. This suggests that the mechanism used in the data analysis was inadequate.

Lii et al.[7] determined k_1 by monitoring [HO_2] and [O_3] following pulse radiolysis of O_2–H_2–Ar mixtures at 1200-torr total pressure. Computer simulations of the observed concentration vs. time profiles were used to obtain a value in good agreement with the present results. However, variation of k_1 from 3.2×10^{-11} to 7.3×10^{-11} cm^3 molecule^{-1} s^{-1} in the simulations had only a small effect on the calculated profiles. Thus, under the conditions used by Lii et al., this approach cannot be used to determine k_1 within error limits less than a factor of 5–10.

Temperature Dependence of k_1. Very few studies of reaction 1 at temperatures other than room temperature have been reported previously. Work by Peeters and Mahnen on methane–oxygen flames resulted in a value for $k_1 \approx 8 \times 10^{-11}$ cm^3 molecule^{-1} s^{-1} at 1600 K.[22] Following studies of H_2–N_2–O_2 flames, Day et al. reported $k_1 = 6 \times 10^{-11}$ cm^3 molecule^{-1} s^{-1} at 1050 K.[23] The present study is the first direct measurement of k_1 at temperatures characteristic of the upper atmosphere. The slightly negative temperature dependence observed in k_1 has also been found in a number of other atom (radical)–radical reactions including reaction 2. Possible interpretations of this temperature dependence have been discussed in detail previously.[24,25]

Atmospheric Chemistry. The present results are expected to have a significant effect on predicted concentrations of atomic oxygen and O_3 in the atmosphere. Reaction 1 is a major loss of atomic oxygen in the upper mesosphere above 65–70 km where loss by reaction with O_2 (eq 43) no longer dominates. Reactions 1 and 2 as well

$$O + O_2 + M \rightarrow O_3 + M \quad (43)$$

as reactions 11 and 14 are important sinks for odd oxygen throughout the mesosphere and upper stratosphere, and, thus, limit the total [O] + [O_3] in these regions. Moreover, reactions 1 and 2 strongly affect the relative concentrations of odd hydrogen species (H, OH, HO_2) in the mesosphere. For example, the concentration ratio [OH]/[HO_2] in this region is given by eq VI,[1] where k_{44} is the rate coefficient

$$\frac{[OH]}{[HO_2]} = \left\{\frac{k_{44}[M][O_2] + k_{14}[O_3]}{k_{44}[M][O_2]}\right\}\frac{k_1}{k_2} \quad (VI)$$

for reaction of atomic hydrogen with O_2 (eq 44). When

$$H + O_2 + M \rightarrow HO_2 + M \quad (44)$$

numerical values are used, it can be shown that the expression in brackets ranges from 1.1 to 1.3 between 40 and 80 km. Thus, to a good approximation, [OH]/[HO_2] is determined by the rate constant ratio k_1/k_2. Previous values used in atmospheric models gave k_1/k_2 near 1.0. With the present results and the recently reported temperature-dependent studies of k_2,[24,25] the ratio increases to 1.9–2.1 between 40 and 80 km. Further work is planned to directly measure k_1/k_2 over a temperature range characteristic of the upper atmosphere.

Acknowledgment. The research described in this paper was performed at the Jet Propulsion Laboratory, California Institute of Technology, under contract with the National Aeronautics and Space Administration.

Appendix

Computer simulations were run to test for interference from secondary reactions and for loss of radicals during the HO_2 to OH conversion. Table VI summarizes the reactions and rate constants used in the simulations.

(20) Sridharan, V. C.; Reimann, B.; Kaufman, F. *J. Chem. Phys.* **1980**, *73*, 1286.
(21) Wine, P. H.; Semmes, D. H.; Ravishankara, A. R. *J. Chem. Phys.* **1981**, *75*, 4390.
(22) Peeters, J.; Mahnen, G. *Symp. (Int.) Combust., [Proc.]* **1972**, *14*, 133.
(23) Day, M. J.; Thompson, K.; Dixon-Lewis, G. *Symp. (Int.) Combust., [Proc.]* **1972**, *14*, 47.
(24) Lewis, R. S.; Watson, R. T. *J. Phys. Chem.* **1980**, *84*, 3495.
(25) Howard, M. J.; Smith, I. W. M. *J. Chem. Soc., Faraday Trans. 2* **1981**, *77*, 997.
(26) DeMore, W. B.; Stief, L. J.; Kaufman, F.; Golden, D. M.; Hampson, R. F.; Kurylo, M. J.; Margitan, J. J.; Molina, M. J.; Watson, R. T. JPL Publication 81-3, 1981, Jet Propulsion Laboratory, California Institute of Technology, Pasadena, CA.
(27) Baulch, D. L.; Cox, R. A.; Hampson, R. F., Jr.; Kerr, J. A.; Troe, J.; Watson, R. T. *J. Phys. Chem. Ref. Data* **1980**, *9*, 295.
(28) Hampson, R. F. Federal Aviation Administration Report No. FAA-EE-80-17, 1980, Washington, DC.
(29) Keil, D. G.; Tanzawa, T.; Skolnik, E. G.; Klemm, R. B.; Michael, J. V. *J. Chem. Phys.* **1981**, *75*, 2693.
(30) Leu, M. T.; Lin, C. L. *Geophys. Res. Lett.* **1979**, *6*, 425.
(31) Clark, J. H.; Moore, C. B.; Reilly, J. P. *Int. J. Chem. Kinet.* **1978**, *10*, 427.
(32) Veyret, B.; Lesclaux, R. *J. Phys. Chem.* **1981**, *85*, 1918.